Myosin-X functions in polarized epithelial cells

Katy C. Liu, Damon T. Jacobs*, Brian D. Dunn†, Alan S. Fanning, and Richard E. Cheney
Department of Cell and Molecular Physiology, School of Medicine, University of North Carolina at Chapel Hill, Chapel Hill, NC 27599

ABSTRACT **Myosin-X (Myo10) is an unconventional myosin that localizes to the tips of filopodia and has critical functions in filopodia. Although Myo10 has been studied primarily in nonpolarized, fibroblast-like cells, Myo10 is expressed in vivo in many epithelia-rich tissues, such as kidney. In this study, we investigate the localization and functions of Myo10 in polarized epithelial cells, using Madin-Darby canine kidney II cells as a model system. Calcium-switch experiments demonstrate that, during junction assembly, green fluorescent protein–Myo10 localizes to lateral membrane cell–cell contacts and to filopodia-like structures imaged by total internal reflection fluorescence on the basal surface. Knockdown of Myo10 leads to delayed recruitment of E-cadherin and ZO-1 to junctions, as well as a delay in tight junction barrier formation, as indicated by a delay in the development of peak transepithelial electrical resistance (TER). Although Myo10 knockdown cells eventually mature into monolayers with normal TER, these monolayers do exhibit increased paracellular permeability to fluorescent dextrans. Importantly, knockdown of Myo10 leads to mitotic spindle misorientation, and in three-dimensional culture, Myo10 knockdown cysts exhibit defects in lumen formation. Together these results reveal that Myo10 functions in polarized epithelial cells in junction formation, regulation of paracellular permeability, and epithelial morphogenesis.**

Monitoring Editor
Alpha Yap
University of Queensland

Received: Apr 25, 2011
Revised: Mar 2, 2012
Accepted: Mar 7, 2012

INTRODUCTION

Myosin-X (Myo10) is an unconventional myosin that is broadly expressed in vertebrate tissues (Berg *et al.*, 2000; Kerber and Cheney, 2011). Myo10 has key functions in filopodia, and experiments with fibroblast-like cells have revealed that Myo10 localizes to the tips of filopodia and undergoes intrafilopodial motility (Berg and Cheney, 2002; Kerber *et al.*, 2009; Watanabe *et al.*, 2010). Importantly, overexpression of Myo10 induces filopodia, while knockdown of Myo10 inhibits the formation of filopodia (Berg and Cheney, 2002; Bohil *et al.*, 2006). Knockdown of Myo10 also inhibits the formation of invadopodia (Schoumacher *et al.*, 2010), actin-based extensions involved in the spread of cancer cells. Although mRNA and blotting studies indicate that Myo10 is expressed at highest levels in epithelia-rich tissues, such as kidney (Berg *et al.*, 2000), very little is known about the localization and functions of Myo10 in polarized epithelial cells.

Myo10 is a member of the myosin tail homology 4 domain and band 4.1/ezrin/radixin/moesin domain (MyTH4-FERM) family of myosins, a phylogenetically ancient group of actin-based motor proteins that have key functions in membrane–cytoskeleton interactions (Breshears *et al.*, 2010; Sousa and Cheney, 2005). The ~237-kDa Myo10 heavy chain can be divided into three regions: a myosin head with motor activity (Kovacs *et al.*, 2005; Nagy *et al.*, 2008; Sun *et al.*, 2010), a neck consisting of three IQ motifs that bind calmodulin or calmodulin-like light chains, and a large tail. The Myo10 tail includes three pleckstrin homology domains, one of which can bind to phosphatidylinositol-3,4,5-trisphosphate (PIP_3; Mashanov *et al.*, 2004; Plantard *et al.*, 2010; Lu *et al.*, 2011). Binding to PIP_3 targets Myo10 to phagosomes (Cox *et al.*, 2002) and has recently been reported to facilitate targeting to filopodia (Plantard *et al.*, 2010; Lu *et al.*, 2011; Umeki *et al.*, 2011). The

This article was published online ahead of print in MBoC in Press (http://www.molbiolcell.org/cgi/doi/10.1091/mbc.E11-04-0358) on March 14, 2012.

Present addresses: *Kidney Institute, Medical Center, University of Kansas, Kansas City, KS 66160; †Department of Biology, Augusta State University, Augusta, GA 30904.

Address correspondence to: Richard E. Cheney (cheneyr@med.unc.edu).

Abbreviations used: AJC, apical junctional complex; AQP1, aquaporin-1; AQP2, aquaporin-2; CLP, calmodulin-like protein; DAPI, 4′,6-diamidino-2-phenylindole; GFP, green fluorescent protein; IgG, immunoglobulin G; MDCK, Madin-Darby canine kidney; Myo10, Myosin-X; MyTH4-FERM, myosin tail homology 4 domain and band 4.1/ezrin/radixin/moesin domain; NA, numerical aperture; NS, nonsilencing; PBS, phosphate-buffered saline; PIP_3, phosphatidylinositol-3,4,5-trisphosphate; RNAi, RNA interference; shRNA, short hairpin RNA; TER, transepithelial electrical resistance; TIRF, total internal reflection fluorescence; ZO-1, zonula occludens-1.

structure of the MyTH4-FERM region was recently solved (Wei *et al.*, 2011), and it has been shown that this region of Myo10 can bind directly to microtubules (Weber *et al.*, 2004) and that Myo10 is required for normal spindle positioning and orientation (Weber *et al.*, 2004; Toyoshima and Nishida, 2007; Kwon *et al.*, 2008; Woolner *et al.*, 2008). The FERM domain of Myo10 can bind the cytoplasmic domains of β1, β3, and β5 integrins (Zhang *et al.*, 2004), important transmembrane receptors for extracellular matrix components. It should also be noted that the neck domain of Myo10 binds to calmodulin-like protein (CLP), an epithelia-specific, calcium-binding protein that can function as a Myo10 light chain (Bennett *et al.*, 2007).

Epithelial cells have critical functions in normal physiology and disease, and epithelial morphogenesis is required for the proper development of tissues and organs. In tissues such as kidney, the epithelium of a tubule is organized into a single layer of polarized cells. The polarity of the epithelial cell is defined by the apical and basolateral domains, with the apical domain facing the lumen, and the basolateral domain contacting the extracellular matrix. The two domains are separated by the apical junctional complex (AJC), the major components of which are the adherens junction and the tight junction. The adherens junction promotes cell–cell adhesion and coordinates changes in cell shape during morphogenesis of tissues and organs (Perez-Moreno *et al.*, 2003). Cadherins, which are calcium-dependent, homophilic, cell adhesion receptors located in the basolateral domain, are a key component of the adherens junction. Cadherins at the adherens junction are linked to actin filaments by scaffolding proteins, such as the catenins (Harris and Tepass, 2010). The tight junction (also known as the zonula occludens) is located immediately above the adherens junction and provides a paracellular barrier to the movement of ions and solutes between cells. The first protein to be identified at the tight junction was zonula occludens-1 (ZO-1; Stevenson *et al.*, 1986), a cytoplasmic scaffolding protein that has important functions in tight junctions. In addition, over 40 proteins are now known to associate with the tight junction (Schneeberger and Lynch, 2004; Shen *et al.*, 2011) including the claudins, transmembrane proteins that are major elements of the tight junction strands that form the paracellular barrier (Van Itallie and Anderson, 2006).

It is now theorized that the paracellular barrier includes at least two pathways (Anderson and Van Itallie, 2009), and different methods are used to measure the integrity of the tight junction barrier and to distinguish between these pathways. Small pores in the tight junction allow some charged ions to pass, and the transepithelial electrical resistance (TER) of an epithelial monolayer provides an instantaneous measurement of this paracellular barrier to ion movement (Anderson and Van Itallie, 2009). The second pathway, termed the "leak" pathway, allows for the passage of larger solutes, and this permeability can be measured as the cumulative paracellular movement (flux) of a solute, such as dextran, over time. Although changes in electrical resistance and solute flux often coincide, it is now apparent that the two pathways can be independently regulated (Balda *et al.*, 1996; Anderson and Van Itallie, 2009; Van Itallie *et al.*, 2009). Because the pores in tight junctions are too small to allow for passage of large solutes, permeability to larger solutes is thought to be due to a different mechanism, such as relatively slow rearrangements of the tight junction strands (Anderson and Van Itallie, 2009; Shen *et al.*, 2011).

The actin cytoskeleton serves as an important structural scaffold for the formation and function of the apical junctional complex (Hirokawa and Tilney, 1982; Hirokawa *et al.*, 1983; Zhang *et al.*, 2005). Ultrastructural studies show that actin filaments associate with both the adherens junction and the tight junction; at the adherens junction, the cadherin-based, cell–cell contacts are clearly associated with a circumferential bundle of actin filaments (Hirokawa and Heuser, 1981; Hirokawa and Tilney, 1982; Hirokawa *et al.*, 1983). Importantly, changes to the actin cytoskeleton can regulate paracellular permeability (Madara, 1998; Hartsock and Nelson, 2008); for example, there is evidence that contraction of actin bundles at the zonula adherens may modulate paracellular permeability (Shen *et al.*, 2006).

While conventional myosin II has been shown to have important roles in junction assembly, permeability, and epithelial morphogenesis (Ivanov *et al.*, 2004, 2007, 2008; Shewan *et al.*, 2005; Smutny *et al.*, 2010), growing evidence indicates unconventional myosins also have critical functions in these processes. Mutations in Myo5b cause microvillar inclusion disease (Muller *et al.*, 2008) and Myo5b has recently been implicated in apical membrane trafficking and lumen formation during epithelial morphogenesis (Roland *et al.*, 2011). Myo6 has been shown to regulate polarized trafficking (Au *et al.*, 2007) and E-cadherin adhesion at epithelial cell–cell contacts (Maddugoda *et al.*, 2007; Mangold *et al.*, 2011). Mutations in Myo7a and Myo15a, two MyTH4-FERM myosins distantly related to Myo10, lead to defects in the stereocilia on the apical surfaces of the inner-ear hair cells and cause human deafness (Friedman *et al.*, 1995; Liu *et al.*, 1997). Myo9a, an unconventional myosin that acts as a Rho-GAP, is reported to localize to cell junctions, and loss of Myo9a leads to defects in epithelial differentiation and to hydrocephalus (Abouhamed *et al.*, 2009). Finally, recent work with Dachs, an unconventional myosin in fly, indicates that that this myosin generates tension in cell–cell junctions and is involved in spindle orientation (Mao *et al.*, 2011).

Although Myo10's functions in the filopodia of nonpolarized cells have been the subject of intensive study, its localization and functions in polarized epithelial cells remain largely unknown. In this paper, we show that Myo10, an unconventional myosin that is broadly expressed in epithelial tissues, has important functions in tight junction biogenesis, the maintenance of paracellular permeability, and epithelial morphogenesis.

RESULTS

Myo10 localizes to the basolateral domain in kidney tubules

To investigate the functions of Myo10 in polarized epithelial cells, we first asked where Myo10 localizes in kidney cells in vivo. Kidney is one of the tissues that expresses the highest levels of Myo10, although it should be noted that Myo10 is a low-abundance protein and that even in the kidney, it is estimated to constitute only ~0.0005% of total protein (Berg *et al.*, 2000). Immunofluorescence of kidney sections from adult mouse showed that anti-Myo10 labels a subset of tubules (Figure 1). To identify the types of tubules that express Myo10, we double-labeled sections with antibodies to aquaporin-2 (AQP2), an apical integral membrane protein selectively expressed in connecting tubules and collecting ducts (Nielsen *et al.*, 2002). Because all AQP2-positive tubules were also labeled by Myo10 (Figure 1A), this indicated that Myo10 is expressed both in connecting tubules, an element of the distal nephron, and in the subsequent collecting ducts. Strikingly, although AQP2 showed its expected apical localization, Myo10 was largely basolateral (Figure 1B). The basal Myo10 staining often appears to extend into the cytoplasm, potentially due to the numerous infoldings of the basal plasma membrane present in renal tubules (Kaissling and Kriz, 1992). Also, anti-Myo10 did stain renal vasculature (unpublished data), consistent with previously reported expression in endothelial cells (Pi *et al.*, 2007). Because some Myo10-positive tubules were not

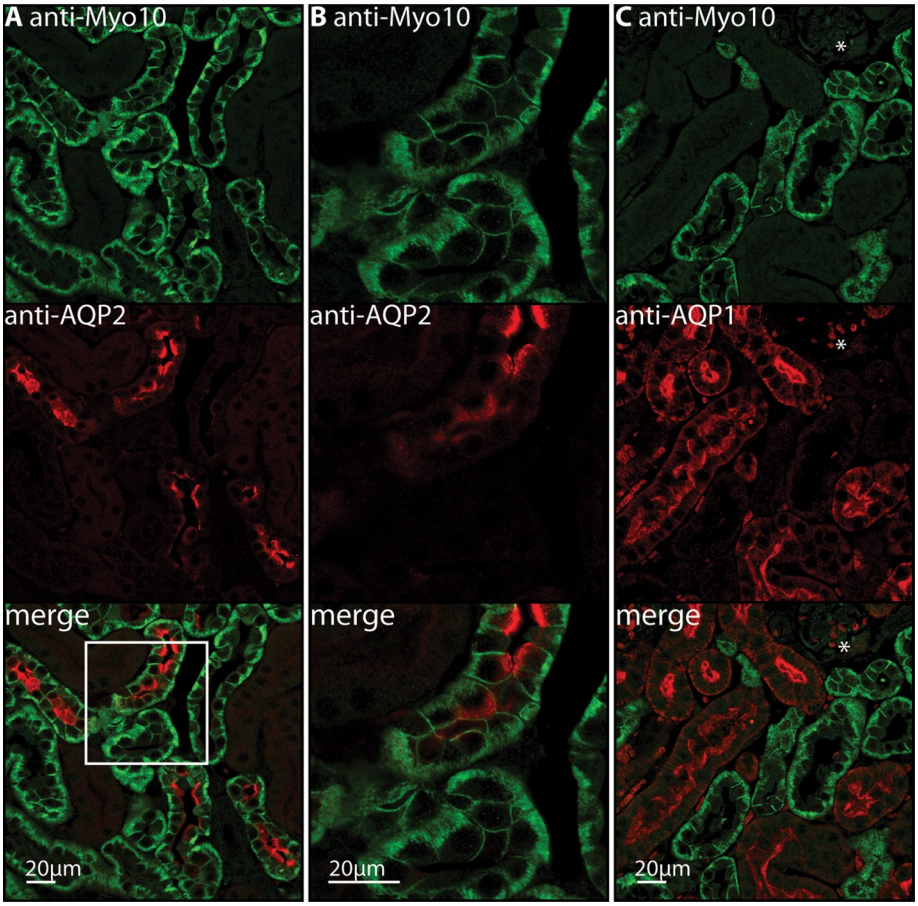

FIGURE 1: Myo10 localizes basolaterally in kidney. (A) Anti-Myo10 antibody labels the basolateral domain in several types of tubules in the renal cortex. These include connecting tubules and collecting ducts, which are labeled by AQP2, an apical protein. (B) A magnified image of the inset box details Myo10's basolateral localization. (C) Little or no Myo10 signal is detected in proximal tubules (labeled with AQP1, red) or in glomeruli (asterisks).

labeled by AQP2, we also performed double-label experiments with aquaporin-1 (AQP1) to determine whether Myo10 is expressed in proximal tubules (Nielsen *et al.*, 2002). No colocalization of Myo10 and AQP1 was detected (Figure 1C), indicating little or no Myo10 is expressed in proximal tubules, a region with an extensive brush border and numerous apical microvilli (Booth and Kenny, 1976). Relatively little Myo10 staining was detected in glomeruli (Figure 1C, asterisks). These experiments demonstrate that Myo10 is expressed in connecting tubules and collecting ducts and that Myo10 exhibits a largely basolateral localization in these polarized epithelial cells.

Myo10 localizes to lateral membranes during polarized junction assembly

On the basis of our observations in mouse kidney, we used Madin-Darby canine kidney (MDCK) II cells as a model system to determine the functions of Myo10 in polarized epithelial cells. Immunoblotting showed that Myo10 is expressed in MDCK cells (Figure 2A). Because trial immunofluorescence experiments with antibodies to human Myo10 yielded high background in MDCK cells, for localization studies, we generated MDCK lines that stably express green fluorescent protein–Myo10 (GFP-Myo10) at levels comparable with endogenous Myo10 (Figure 2A). In subconfluent, spreading MDCK cells, GFP-Myo10 localized to the tips of filopodia (Figure 2B), as expected from results in other cell types (Berg and Cheney, 2002).

We then examined the subcellular distribution of GFP-Myo10 in MDCK cells during junction formation. Junction assembly was induced using the calcium-switch assay (Cereijido *et al.*, 1978). In this assay, monolayers of MDCK cells are exposed overnight to low calcium, which disrupts cadherin-dependent, cell–cell adhesion, leading to a loss of cell–cell junctions and cell polarity. Readdition of calcium triggers cell–cell adhesion, and the adherens junctions and tight junctions reassemble over several hours. In many types of epithelial cells, E-cadherin exhibits initial localization to cell–cell contacts that matures into a narrow band at the adherens junction (Boller *et al.*, 1985; Adams *et al.*, 1996); however, in MDCK cells, E-cadherin remains localized throughout the lateral membrane (Gumbiner and Simons, 1987). As junctions reassemble, TER transiently increases to high levels, and then declines over 1–2 d toward the much lower "steady-state" TER of mature monolayers (Gonzalez-Mariscal *et al.*, 1985). After overnight incubation in low-calcium media, MDCK cells had a rounded and unpolarized morphology; GFP-Myo10 localization was diffuse within these cells (Figure 2C). We also found that GFP-Myo10 showed variable levels of expression from cell to cell. On readdition of calcium to trigger junction assembly, GFP-Myo10 showed clear but transient labeling at the lateral membrane of cell–cell contacts, most notably at 2–6 h. The transient localization of GFP-Myo10 to lateral membranes could also be seen in *x,z*-projections (Supplemental Figure S1). By 24 h, the lateral staining of GFP-Myo10 largely disappears (Figure 2G).

Because GFP-Myo10 localized to the lateral membrane during junction assembly, we examined the subcellular distribution of GFP-Myo10 relative to the adherens junction protein E-cadherin. As expected, after incubation in low calcium, E-cadherin showed a diffuse localization in the cytoplasm. Following readdition of calcium, E-cadherin rapidly redistributed to cell–cell contacts and formed adherens junctions. GFP-Myo10 colocalized with E-cadherin at the lateral membrane at 2 and 4.5 h after calcium readdition (Figure 2, E″ and F″). E-cadherin localization to the lateral membrane, however, preceded that of GFP-Myo10; E-cadherin was detected at the lateral membrane at 0.5 h (Figure 2, D and D′).

Like E-cadherin, ZO-1 localization was disrupted after incubation in low calcium and was apparent at cell–cell contacts prior to Myo10 (Figure S2, B and B′). Although both ZO-1 and Myo10 were present in lateral membranes, the distribution of ZO-1 was more focused at the apical junctional complex. In fact, little if any Myo10 was detected in *x,y*-sections at the level of ZO-1 and the apical junction complex (Figure S2, A–E). Thus, although GFP-Myo10 colocalizes with E-cadherin at the lateral membrane during junction assembly, Myo10 is not enriched at the apical junctional complex in MDCK cells. Furthermore, GFP-Myo10 was not detected at the lateral membrane during the initial recruitment of E-cadherin (or ZO-1) to cell junctions.

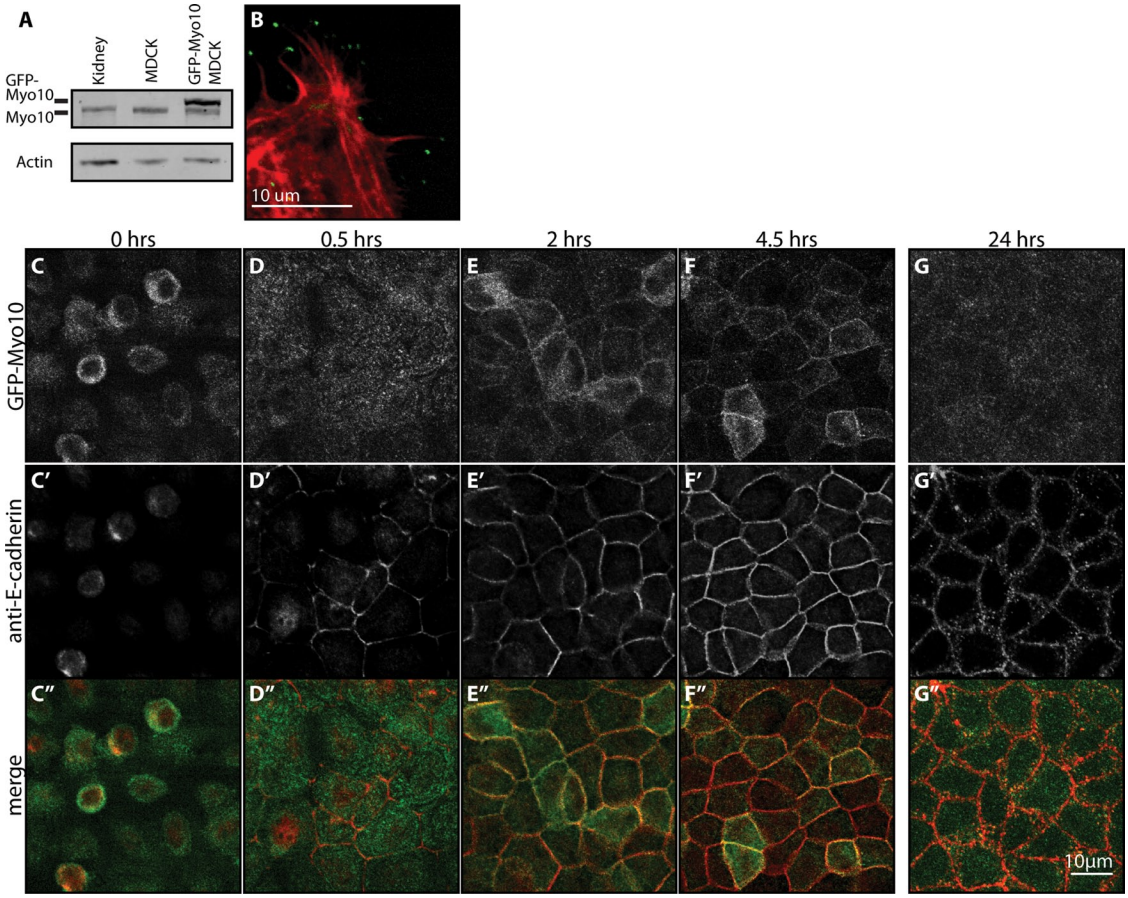

FIGURE 2: GFP-Myo10 localizes to the tips of filopodia in spreading MDCK II cells and to lateral membranes during junction formation. (A) Immunoblot showing expression of Myo10 in mouse kidney, MDCK cells, and MDCK cells stably expressing GFP-Myo10. Actin was used as a loading control. MDCK samples were collected from monolayers after 5 d in culture, and kidney lysates were obtained from adult C57BL/6 mice. (B) GFP-Myo10 (green) localizes to the tips of filopodia in spreading MDCK cells. Cells were fixed 1 d postplating and were also stained for F-actin with Alexa Fluor 568 phalloidin (red). (C–G) GFP-Myo10 transiently localizes to the lateral membrane during junction assembly. After overnight incubation in low calcium to disrupt cell–cell adhesion, cells were rounded and GFP-Myo10 showed a diffuse cortical localization (C). After junction assembly was triggered by readdition of calcium (D–G), GFP-Myo10 was transiently recruited to the lateral membrane, most strongly between 2 and 4.5 h. (C′–G′) Localization of E-cadherin during junction assembly. Note that E-cadherin is present at the lateral membrane at 0.5 h (D′), prior to the recruitment of GFP-Myo10. (C″ –G″) Merged images of GFP-Myo10 (green) and E-cadherin (red). GFP-Myo10 colocalizes with E-cadherin at the lateral membranes at 2 and 4.5 h (E″ and F″). Images (G and G″) from a 24-h time point showing lack of Myo10 staining at lateral membrane in more mature monolayers. Images are single confocal planes taken from the midsection of the cell monolayers.

To investigate the dynamics of Myo10 during junction assembly, we imaged GFP-Myo10 during calcium switch (Supplemental Movie S1). Total internal reflection fluorescence (TIRF) microscopy of the basal surface revealed numerous puncta of GFP-Myo10, many of which localize to the tips of highly dynamic, filopodia-like projections. GFP-Myo10 was present at filopodia-like projections throughout junction assembly, even prior to localization of GFP-Myo10 to lateral membranes.

Myo10 knockdown delays the assembly of E-cadherin and ZO-1 to cell–cell contacts

Given the localization of Myo10 during junction assembly, we tested whether Myo10 has functional roles in junction formation in polarized epithelial cells. Because Myo10 has been efficiently knocked down using RNA interference (RNAi) approaches (Zhang *et al.*, 2004; Bohil *et al.*, 2006; Pi *et al.*, 2007), we established stable Myo10 knockdown lines in MDCK cells using short hairpin RNA (shRNA) constructs. Knockdown of full-length Myo10 was confirmed by immunoblot (Figure 3A), and Myo10 was depleted by ~70–80%. We then used the calcium-switch assay to examine the process of junction assembly in Myo10 knockdown cells. Importantly, Myo10 knockdown cells showed a delay in the recruitment of both E-cadherin and ZO-1 to cell–cell contacts (Figure 4). Most notably, at 2.5 h, E-cadherin and ZO-1 staining was discontinuous or punctate in Myo10 knockdown cells (Figure 4, G and G′), whereas E-cadherin and ZO-1 were organized in a continuous, linear pattern in control MDCK cells (Figure 4, C and C′). Assembly of ZO-1 into continuous, linear contacts was quantified using ImageJ (Arganda-Carreras *et al.*, 2010). Consistent with immunofluorescence studies, Myo10 knockdown cells showed reduced continuous ZO-1 length at all time points until 4.5 h (Figure S3). E-cadherin was properly restricted to the lateral membrane and ZO-1 to the apical junction; therefore knockdown of Myo10 does not appear to affect overall cell polarity. We stained for additional polarity markers, ezrin and gp135, and

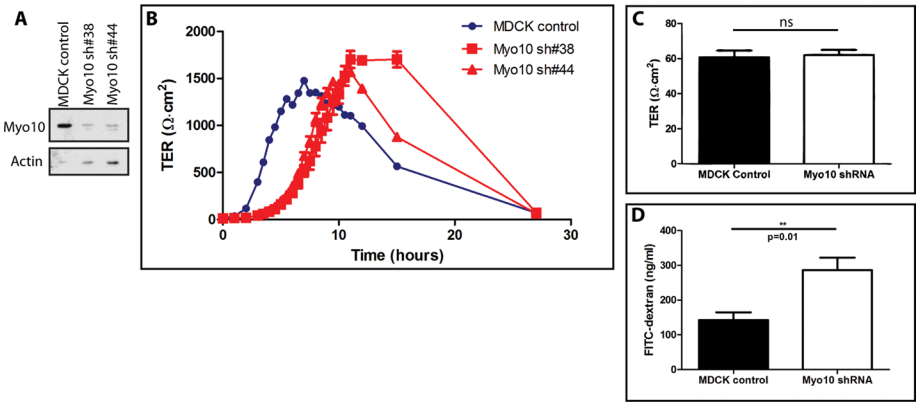

FIGURE 3: Myo10 knockdown delays tight junction formation measured by TER. (A) Immunoblot showing knockdown of Myo10 in stable MDCK lines, sh#38 and #44. Actin was used as a loading control. (B) Myo10 knockdown cells show an ~4-h delay in the timing of the peak TER during the calcium-switch assay, thus demonstrating a kinetic defect in junction formation. By ~28 h, the TER in both control and knockdown cells return to normal levels, ~60 Ω · cm^2. (C) Knockdown of Myo10 does not affect TER in mature monolayers (measured after 5 d in culture). (D) Knockdown of Myo10 does increase paracellular permeability to large solutes in mature monolayers. Cells were cultured for 5 d, then flux assays were performed to measure the movement of 3.0-kDa FITC-dextran over a 2-h time period. Calcium-switch experiments were performed in quadruplicate. Paracellular permeability results were averaged over two experiments. **, p = 0.01; ns, not significant.

their localization was also unchanged in 5-d-old MDCK monolayers with Myo10 knockdown (Figure 5). Also, the localization of polarity protein markers, Par3 and aPKC, in MDCK monolayers grown for 5 d were unaffected by Myo10 knockdown (Figure S4). These and subsequent studies were confirmed with two independent shRNAs (Figure S5).

Loss of Myo10 leads to a delay in tight junction barrier formation as assayed by TER

The delay in localization of E-cadherin and ZO-1 to cell–cell contacts suggested that loss of Myo10 might result in a delay in tight junction barrier function. We thus tested whether loss of Myo10 leads to defects in the formation of the epithelial barrier by measuring TER during junction assembly. As expected for control MDCK cells, TER was low in the absence of calcium; upon readdition of calcium, TER increased substantially and peaked between 6–8 h. Myo10 knockdown cells, however, showed a marked delay in attaining peak TER (Figure 3B). This ~4-h delay to peak TER indicates a defect in the kinetics of tight junction formation, a phenomenon that has also been observed in MDCK cells in which critical tight junction and adherens junction proteins, such as ZO-1 and E-cadherin, have been depleted (McNeil *et al.*, 2006; Capaldo and Macara, 2007).

Although Myo10 knockdown led to a delay in the development of peak TER, by ~28 h, the TER of both knockdown and control cells declined to typical steady-state levels, ~60 Ω · cm^2 (Figure 3B). Knockdown and control cells were also indistinguishable when the TER was assayed after 5 d in culture (Figure 3C). This demonstrates that although Myo10 is required for normal kinetics of junction assembly, it is not necessary for maintenance of TER once junctions have formed. Consistent with the latter point, knockdown of Myo10 in Caco-2 cells (a model for intestinal epithelial cells), also had no effect on the steady-state TER (Figure S6, A and B).

Loss of Myo10 increases paracellular permeability to uncharged solutes

A key feature of epithelial barrier function is the "leak" pathway, which represents the paracellular permeability to large solutes (Anderson and Van Itallie, 2009). This leak pathway for large solutes can be regulated independently of the permeability to small ions that is assayed by TER (Balda *et al.*, 1996) and is most frequently analyzed by measuring the movement of uncharged dextran conjugates across the monolayer. Importantly, paracellular permeability to 3.0-kDa dextran more than doubled in Myo10 knockdown cells (Figure 3D). This demonstrates that, although Myo10 is not required to maintain the permeability barrier to small ions, Myo10 is required to maintain the permeability barrier to large solutes. Myo10's role in regulating permeability is not limited to MDCK cells, since knockdown of Myo10 in Caco-2 cells led to similar results (Figure S6, C and D).

Myo10 is required for proper mitotic spindle orientation

Myo10 can bind to microtubules through its MyTH-FERM domain (Weber *et al.*, 2004), and Myo10 has been shown to be important for spindle formation and length in *Xenopus* (Woolner *et al.*, 2008) and proper spindle orientation in fibroblast-like cells (Toyoshima and Nishida, 2007). Yet, whether Myo10 is required for spindle orientation in polarized epithelial cells is largely unknown. To investigate the role of Myo10 in the spindles of MDCK cells, we fixed mature monolayers and stained for 4′,6-diamidino-2-phenylindole (DAPI) to identify dividing metaphase cells. By costaining for γ-tubulin to identify centromeres, we measured the spindle angle and spindle length, and found that Myo10 knockdown cells showed increased average spindle angle (0° = horizontal) and a wider distribution of spindle angles when compared with control cells (Figure 6, A and B). This defect in spindle orientation is similar to those reported for key proteins required for spindle orientation such as Cdc42 (Jaffe *et al.*, 2008) and cadherins (den Elzen *et al.*, 2009). No difference in average spindle length was detected with Myo10 knockdown (Figure 6C).

Myo10 is required for normal lumen formation in MDCK cysts

Our experiments on two-dimensional MDCK monolayers demonstrated that Myo10 has a role in the formation of adherens and tight junctions as well as in spindle orientation. Because cell junctions and the spindle have been shown to have important roles in epithelial morphogenesis (Krasnow and Nelson, 2002), we tested whether Myo10 is required for morphogenesis of epithelial cysts. We seeded cells at low density in a collagen-matrigel matrix and allowed each cell to grow into a cyst for 6 d before staining with various markers. While the majority (~80%) of control MDCK cells were able to form a single lumen, only ~20–40% of Myo10 knockdown cells formed single lumens and instead showed a striking multi-lumen phenotype (Figure 7, A and B). Although there was a clear defect in lumen formation, Myo10 knockdown cysts did not appear to have defects in the polarized localization of the junctional marker ZO-1, the apical marker gp135, or the basolateral marker E-cadherin (Figure 7, B and D). Similar to what was observed in two-dimensional culture, normal apico-basal polarity was also confirmed by additional markers, including ezrin at the apical domain and Na^+,K^+-ATPase at the basolateral domain (Figure S7).

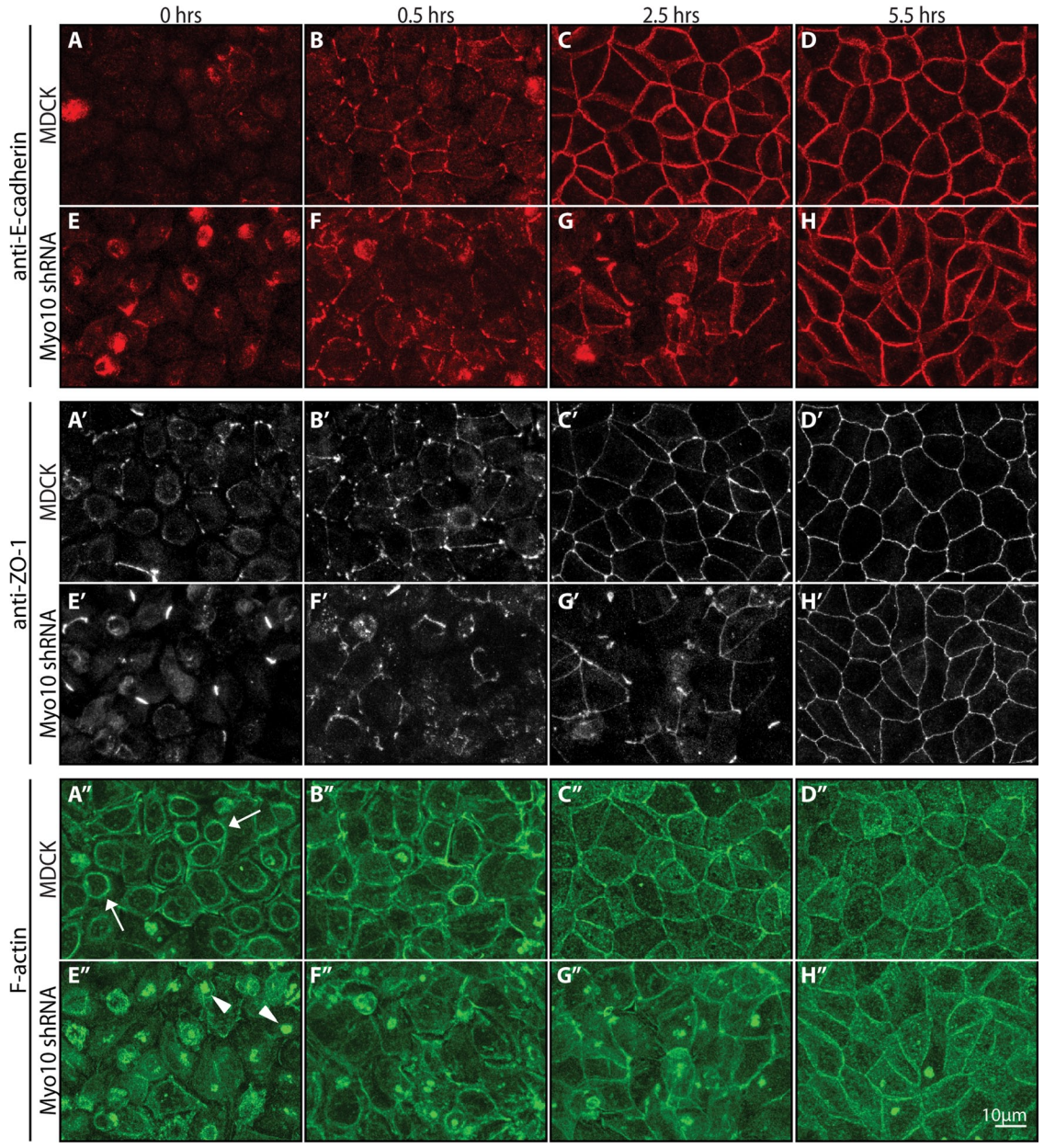

FIGURE 4: Myo10 knockdown delays E-cadherin and ZO-1 localization during junction formation. In calcium-switch experiments, knockdown of Myo10 (sh#44) delays the appearance of E-cadherin (A–H). This is most evident at the 2.5-h time point, at which the cadherin staining in Myo10 knockdown cells shows a more punctate and discontinuous pattern that largely normalizes by 5.5 h. Similar delays were observed with ZO-1 (A′–H′) and F-actin (A″–H″). In control calcium-depleted MDCK cells, concentric actin "rings" were observed (A″, arrows), whereas fewer actin rings and many actin "condensations" were detected in Myo10 knockdown cells at early time points, most notably at t = 0 (E″, arrowheads). All images are maximum projections of confocal Z-stacks with 0.5-μm slice thickness.

Thus Myo10 does not appear to be necessary for establishment of apico-basal polarity, but is required for epithelial morphogenesis to form normal cysts with single lumens.

GFP-Myo10 rescues defects in cyst formation

To confirm that the effect of Myo10 shRNA was specific, we generated Myo10 knockdown lines that stably express bovine GFP-Myo10 and asked whether expression of the transgene rescued the multiple-lumen phenotype. Immunoblotting confirmed the knockdown of endogenous Myo10 and the expression of GFP-Myo10 (Figure 8A). In addition, confocal imaging of rescue cells plated at low density showed GFP-Myo10 labeling at the tips of filopodia (Figure 8B). Rescue cells were plated in collagen-matrigel to assay the efficacy of cyst formation in three-dimensional culture. Although the number of single lumens in control cells was somewhat lower in this series of experiments (~70–75%), GFP-Myo10 expression partially rescued the multi-lumen phenotype of Myo10 knockdown cells (Figure 8E); ~60% of GFP-Myo10 rescue cysts had single lumens, compared with ~35% of Myo10 knockdown cysts. The partial rescue is probably attributable to the heterogeneous expression of GFP-Myo10 in the rescue cells, especially given that some cells exhibited little to no expression of GFP-Myo10, much like the stable GFP-Myo10 cells shown in Figure 2. Apico-basal polarity also remained intact in GFP-Myo10 rescue cysts (unpublished data). To further

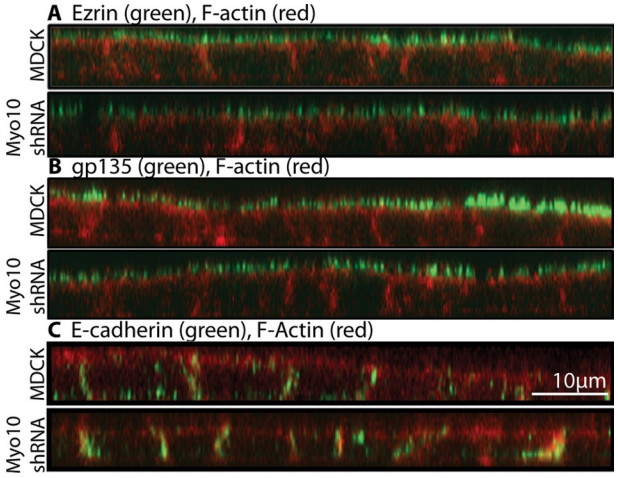

FIGURE 5: Myo10 knockdown does not affect markers of apico-basal polarity in MDCK monolayers. (A and B) Apical markers, ezrin and gp135, localize to the apical microvilli in knockdown (sh#16) and control MDCK cells. (C) E-cadherin localizes to the basolateral membrane in knockdown and control cells. Cells were fixed at 6-d postplating. Confocal images were acquired on a Zeiss 510 LSM using a 63×/1.4 NA Plan-Apochromat oil objective. Sections were acquired every 0.5 μm.

confirm the specificity of the Myo10 knockdown, we generated additional knockdown lines that stably express different shRNAs to Myo10 and confirmed all the phenotypes in junction assembly, paracellular permeability, and cyst formation (Figure S5).

DISCUSSION

Although Myo10 is broadly expressed in epithelial tissues, its functions in polarized epithelial cells have remained largely unknown. In this study, we show that Myo10 has important and unexpected functions in epithelial cells, including junction formation, maintenance of the permeability barrier to large solutes, and epithelial morphogenesis.

Myo10 localizes to the basolateral domain in polarized epithelial cells

While previous work with nonpolarized cells has shown that Myo10 localizes to protrusive structures, such as the tips of filopodia (Berg *et al.*, 2000; Tokuo *et al.*, 2007), the in vivo localization data here from the kidney connecting tubules and collecting ducts show that Myo10 exhibits a largely basolateral distribution in polarized epithelial cells. Given that Myo10 localizes to dorsal filopodia in nonpolarized cells, it is somewhat surprising that Myo10 was not detected in proximal tubules, which have numerous apical microvilli, and that GFP-Myo10 was not detected in the apical microvilli of MDCK cells. This demonstrates that Myo10 is not targeted to the tips of all actin-based bundles and suggests that there are important differences between the dorsal filopodia of nonpolarized cells and the apical microvilli of polarized epithelial cells. Our results showing a basolateral localization of Myo10 are consistent with biochemical fractionation experiments that identified Myo10 in basolateral rather than apical fractions from kidney (Yonezawa *et al.*, 2003). They are also consistent with proteomics data showing that Myo10 was not among the 14 myosins detected in the intestinal brush border (McConnell *et al.*, 2011). Although the precise mechanisms underlying the basolateral localization of Myo10 remain unknown, the Myo10 tail domain binds to PIP_3 and to β integrins, (Mashanov *et al.*, 2004; Zhang

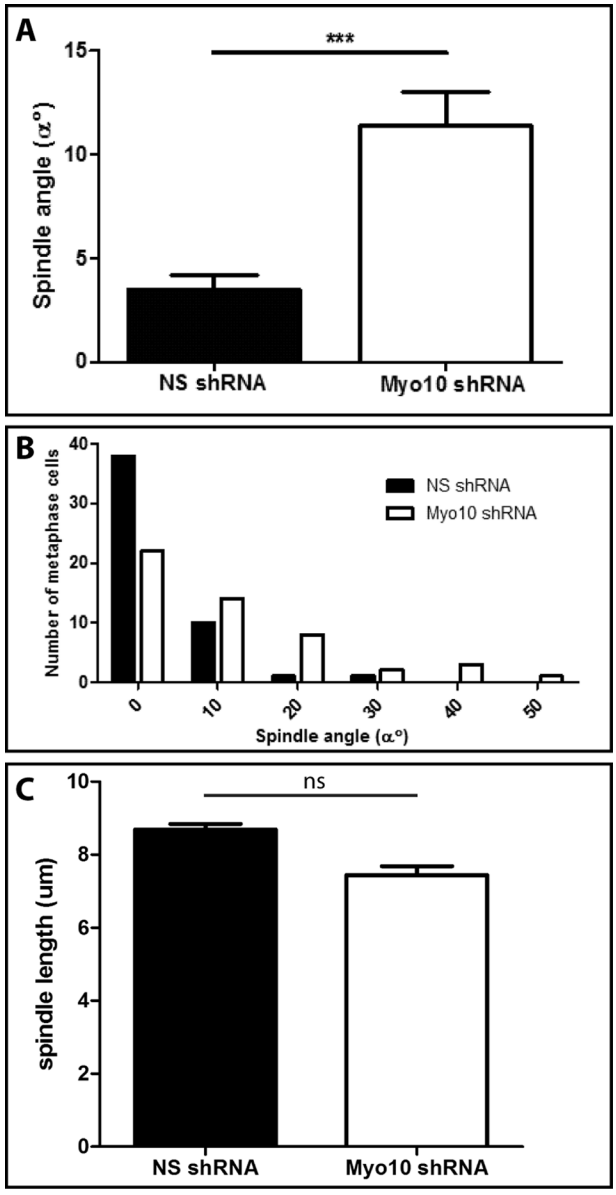

FIGURE 6: Myo10 knockdown cells show a defect in proper spindle orientation, but not spindle length, in mature MDCK monolayers. (A) Myo10 knockdown cells (sh#2–8) show increased average spindle angle from horizontal (0°) and a larger distribution of spindle angles (B) (see Supplemental Material). The histogram in (B) plots the number of metaphase cells with spindle angles binned in 10° increments. (C) Myo10 knockdown has no significant effect on spindle length in MDCK monolayers. Fifty cells/condition were counted. ***, $p < 0.001$; ns, not significant.

et al., 2004; Wei *et al.*, 2011), both of which localize basolaterally in MDCK cells (Schoenenberger *et al.*, 1994; Martin-Belmonte *et al.*, 2007).

Loss of Myo10 delays junction formation

Using MDCK cells and the calcium-switch model, we found that GFP-Myo10 was diffusely distributed within the cell at early stages of junction assembly, and it localized to the lateral membrane as cell–cell contacts formed. More importantly, Myo10 knockdown cells showed a delay in junction formation as indicated by: 1) delays in the localization of E-cadherin and ZO-1 and 2) delay in barrier

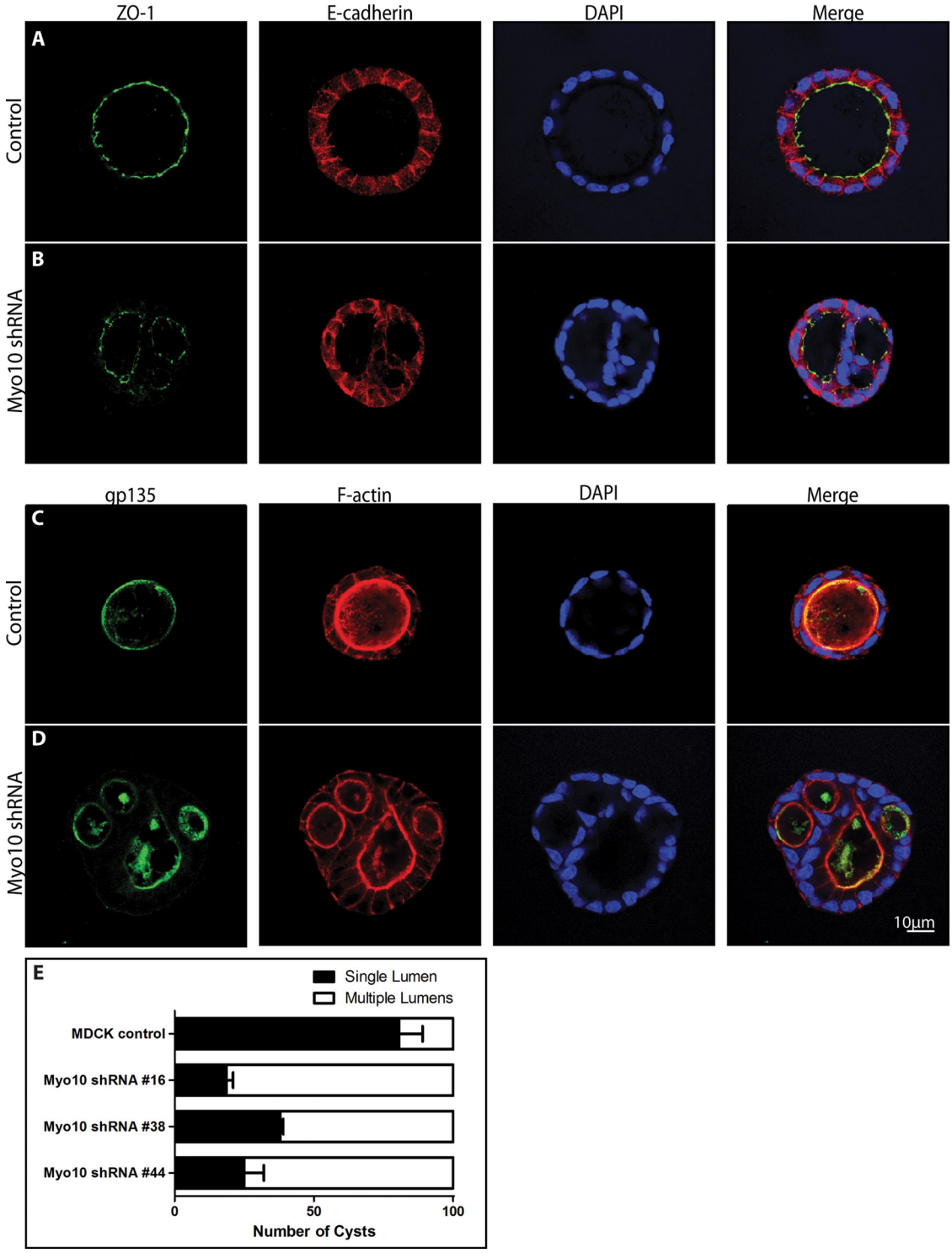

FIGURE 7: Myo10 knockdown leads to the formation of cysts with multiple lumens. (A and C) The majority of control MDCK cells grown in three-dimensional, collagen-matrigel matrix for 6 d form cysts with a single lumen, whereas the majority of Myo10 knockdown cells (sh#44) form cysts with multiple lumens (B and D). Cysts were stained for the tight junction marker ZO-1, the basolateral marker E-cadherin, and the apical markers gp135 and F-actin, as well as DAPI to stain for nuclei. Myo10 knockdown cells retain apico-basal polarity, as the apical and basolateral markers localize to their proper domains. (E) Bar diagrams showing the number of cysts with single versus multiple lumens, ascertained from 100 randomly selected cysts per condition and averaged over two experiments. While ~80% of control MDCK cells form single-lumen cysts, only ~20–40% of Myo10 knockdown cells form single-lumen cysts. Statistical significance ($p < 0.05$) was achieved between MDCK vs. sh#16, MDCK vs. sh#38, and MDCK vs. sh#44.

function, as indicated by the ~4-h delay to reach peak TER. The delay in junction formation was temporary, and knockdown cells exhibited normal TER by ~28 h. Knockdown of Myo10 thus leads to defects remarkably similar to those resulting from loss of key junction components, such as E-cadherin and ZO-1, loss of either of which leads to similar delays in junction formation and TER without

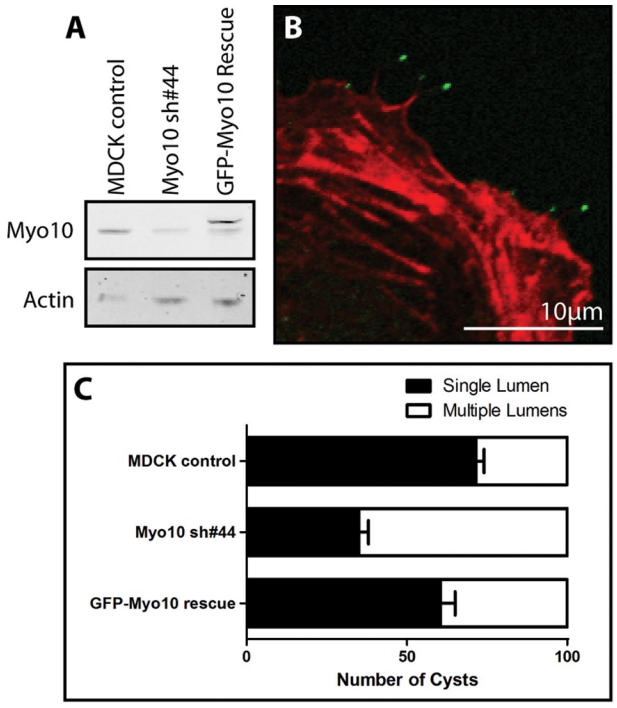

FIGURE 8: Partial rescue of multiple-lumen cyst phenotype by expression of GFP-Myo10. (A) Immunoblot showing knockdown and rescue of Myo10 expression in MDCK lines. Antiactin is shown as a loading control. (B) Fluorescence image of a rescue MDCK cell during spreading shows that GFP-Myo10 (green) localizes to filopodia tips as expected for functional Myo10; F-actin (red) was stained with phalloidin. (C) Myo10 knockdown (sh#44) increased the number of cysts with multiple lumens relative to control cells, and expression of GFP-Myo10 partially rescued this defect. Statistical significance ($p < 0.05$) was achieved for MDCK vs. sh#44 and sh#44 vs. GFP-Myo10 rescue.

affecting steady-state TER (Umeda *et al.*, 2004; McNeil *et al.*, 2006; Capaldo and Macara, 2007).

Loss of Myo10 could delay junction formation by several mechanisms. It has been proposed that nascent junctions in keratinocytes form by filopodial contacts between adjacent cells (Vasioukhin *et al.*, 2000). Because we observed Myo10 at the tips of filopodia in unpolarized MDCK cells, Myo10 is well-positioned to facilitate the formation of initial cell–cell contacts. Furthermore, TIRF microscopy revealed that GFP-Myo10 localizes to the tips of filopodia-like structures at the basal surface of MDCK monolayers; these basolateral puncta of GFP-Myo10 were very dynamic (Movie S1). The data illustrating GFP-Myo10 at the tips of filopodia-like structures suggest a mechanism whereby Myo10 functions in junction formation by affecting filopodial cell–cell contacts. A similar role has recently been suggested for Myo10 in endothelial cells, in which Myo10 transiently colocalized with VE-cadherin at the tips of filopodia during the initial stages of cell–cell contact (Almagro *et al.*, 2010). This suggested that knockdown of Myo10 might impair junction formation, although this was not tested. In this study, we directly show that knockdown of Myo10 leads to a delay in junction formation. Because it is reasonable to suspect that the role of Myo10 in junction formation could be due to an interaction with E-cadherin, we performed series of preliminary immunoprecipitation experiments, both during calcium-switch and in mature monolayers, but did not detect an interaction between Myo10 and E-cadherin (unpublished data).

As an actin-based motor, Myo10 could potentially transport or localize proteins involved in junction formation. Although E-cadherin was detected at lateral membranes prior to GFP-Myo10, E-cadherin localization to the lateral membrane was delayed in Myo10 knockdown cells. This suggests that loss of Myo10 leads to delays at an earlier step, such as formation of initial contacts, or that amounts of Myo10 too low for us to detect are sufficient to localize E-cadherin to lateral membranes. The normal apico-basal polarity observed in Myo10 knockdown cells suggests that Myo10 is not essential for pathways required for polarized membrane trafficking.

It is also possible Myo10 is required to properly regulate actin dynamics at cell junctions. Interestingly, we observed differences in actin morphology with Myo10 knockdown, most notably in calcium-depleted cells. While F-actin formed apical ring-like structures in control cells (Figure 4A″, arrows), as previously described (Ivanov *et al.*, 2004), Myo10 knockdown cells showed fewer apical F-actin rings and more F-actin "condensations" within the cells (Figure 4E″ arrowheads). On calcium readdition, actin condensations could be observed at early stages (0.5–2 h), but by 5.5 h and in mature monolayers, the Myo10 knockdown cells exhibited apparently normal actin organization. Although the nature of the actin condensations is not clear, similar actin structures have been reported in cells knocked down for ZO-1 (McNeil *et al.*, 2006). It is thus possible that Myo10 knockdown delays junction assembly by perturbing actin organization, especially given that myosin II and Myo6 are involved in the assembly of junctions and associated actin structures (Ivanov *et al.*, 2007; Ivanov, 2008; Smutny *et al.*, 2010; Mangold *et al.*, 2011).

Loss of Myo10 results in increased paracellular permeability

Myo10 knockdown monolayers showed increased movement of dextran solute through the paracellular pathway over a period of 2 h. This finding indicates that Myo10 is required for maintenance of the paracellular barrier. Although the mechanisms underlying the paracellular "leak" pathway are unclear, the actin cytoskeleton is integral in retaining the paracellular barrier (Shen *et al.*, 2011). It is thus possible that Myo10 is required for cytoskeletal organization or dynamics that are necessary to maintain normal paracellular flux. Although Myo10 was not enriched at the tight junction, other proteins that localize outside the tight junction, such as E-cadherin, have been shown to affect paracellular permeability in MDCK cells (Capaldo and Macara, 2007).

Loss of Myo10 increases paracellular permeability, but at the same time, it does not affect steady-state TER. How can this be reconciled? TER and paracellular permeability are not necessarily coupled. This has been shown in several cases (Balda *et al.*, 1996; McCarthy *et al.*, 2000; Bruewer *et al.*, 2004), most recently in ZO-1 knockdown in MDCK cells, in which steady-state TER is unchanged and paracellular flux is increased (Van Itallie *et al.*, 2009; Fanning *et al.*, 2012). It has been theorized that the highly dynamic tight junction fibrils act akin to a series of gates (Claude, 1978), in which the opening and closing of tight junction fibrils allow solute particles to progress through the paracellular pathway over time. Thus, while TER is an instantaneous, static reading of the epithelial barrier to small ions, paracellular flux is a time-dependent, dynamic measurement of the barrier to larger solutes.

Myo10 is needed for normal lumen formation in epithelial morphogenesis

In three-dimensional culture, Myo10 knockdown leads to a dramatic increase in the number of cysts with multiple lumens. Defects in several different pathways can result in a multiple-lumen phenotype, including establishment of apico-basal polarity (Shin *et al.*, 2005;

Schluter *et al.*, 2009) or mitotic spindle orientation (Jaffe *et al.*, 2008). Apico-basal polarity can be established by polarity proteins, and the loss of polarity proteins such as Crumbs3 gives rise to multiple lumens or an absence of lumens in three-dimensional cysts (Shin *et al.*, 2005; Schluter *et al.*, 2009). Disruption of the normally basolateral PIP_3 localization in MDCK cells also results in cysts with multiple lumens (Martin-Belmonte *et al.*, 2007). Because Myo10 binds PIP_3 (Plantard *et al.*, 2010; Lu *et al.*, 2011; Umeki *et al.*, 2011), it may act downstream of PIP_3 in cyst morphogenesis.

Myo10 could also act via its involvement in spindle orientation, since spindle misorientation can lead to multi-lumen cysts, as demonstrated with Cdc42 knockdown (Jaffe *et al.*, 2008) as well as Tuba and Par3 knockdown (Hao *et al.*, 2010; Qin *et al.*, 2010). Consistent with this, we show that Myo10 knockdown leads to defects in spindle orientation in MDCK monolayers (Figure 6). Although Woolner *et al.* (2008) report that morpholino-mediated knockdown of Myo10 in *Xenopus* embryos led to an ~35% increase in spindle length, we did not detect changes in spindle length in Myo10-knockdown MDCK cells. This may reflect differences in species, cell type, or method of knockdown. Whereas Toyoshima and Nishida (2007) showed that Myo10 is required for spindle orientation in unpolarized HeLa cells, a process that depends on integrin-based, cell-substrate adhesions, our work reveals that Myo10 is also required for spindle orientation in polarized epithelial cells, in which the cues for spindle orientation are thought to be provided, at least in part, by cell–cell contacts.

Together our results demonstrate important and unexpected roles for Myo10 in polarized epithelial cells. The phenotypes we observed in tight junction formation and epithelial morphogenesis were similar to those observed with critical junctional proteins, such as E-cadherin and ZO-1, and indicate that it will be important for future studies to investigate Myo10's precise mechanisms of action and its functions in vivo.

MATERIALS AND METHODS

Cell culture and plasmids

MDCK II Tet-Off cells (Clontech, Mountain View, CA), referred to as "MDCK," were grown in complete media: DMEM high-glucose (Life Technologies/Invitrogen, Carlsbad, CA) with 10% fetal bovine serum (Life Technologies) and 100 U/ml penicillin–streptomycin (Sigma-Aldrich, St. Louis, MO). MDCK cells were maintained at 37°C and 5% CO_2 and were passaged every 5 d.

Plasmids

Canine Myo10 shRNA constructs were generated by cloning Myo10 shRNA (target sequences GGAGAAGAACAGAGATACA [sh#2]; GGAAAGGAATTATCACATA [sh#4]; and GGAGATGCATCACTGGATA [sh#5]) into the *Bgl*II/*Hin*dIII sites of the pSuper vector (Oligoengine, Seattle, WA). The nonsilencing (NS) shRNA construct was generated by cloning a nonspecific shRNA (GATCGACTTACGACGTTAT) into the pSuper vector. To generate Myo10 knockdown or NS shRNA-expressing cell lines, we plated MDCK cells at 150×10^4 cells per 10-cm dish. After overnight incubation, 2 μg Myo10 shRNA (pool of Myo10 shRNAs #2 and #4) and 0.2 μg pBLAST49 with blasticidin resistance (InvivoGen, San Diego, CA) were cotransfected using 41 μl lipofectamine 2000 (Invitrogen). Cells were incubated for 3 d and plated at different dilutions into 15-cm dishes. Clonal cell lines were selected by antibiotic resistance using complete media with 10 μg/ml blasticidin (InvivoGen). Myo10 shRNA cell lines #16, 38, and 44 are clones of pooled Myo10 shRNAs, as described above. All results were confirmed using two independent Myo10 shRNAs, sh#2 (clone 8) and sh#5 (clones 16, 35).

Because the antibodies to human Myo10 exhibited high background in immunofluorescence experiments with MDCK cells, we generated MDCK cells stably expressing a GFP-Myo10 plasmid. The GFP-Myo10 plasmid (BD71) contains an enhanced GFP-1xFLAG tag at the N-terminus of full-length bovine Myo10 (aa 1–2052) and a Spe1 site immediately 5′ to the Myo10 stop codon. The GFP-Myo10 is expressed by a pSNAPtag(m) (New England Biolabs, Ipswich, MA) vector that was modified by deleting the SNAP tag while retaining the vector's internal ribosome entry site for expression of neomycin resistance in mammalian cells. MDCK II cells were transfected with the BD71 GFP-Myo10 by nucleofection using conditions optimized for MDCK II cells (Lonza, Basel, Switzerland). Clonal stable cell lines (#3) were selected using 0.9 mg/ml G418 (Sigma-Aldrich). Expression of GFP-Myo10 was confirmed by immunoblot.

For demonstration that the knockdown effects were specific, stable knockdown cells were stably rescued by cotransfection with 2 μg GFP-Myo10 (BD71) and 0.1 μg pSVZeo (Invitrogen) by Amaxa nucleofection Kit L using conditions optimized for MDCK II cells. Clonal cell lines (#7) were selected using 1 mg/ml Zeocin (InvivoGen). Expression of GFP-Myo10 was confirmed by immunoblot.

Immunofluorescence microscopy and immunoblotting

Antibodies used were: rabbit anti–human Myo10 (HPA024223; Sigma-Aldrich), mouse anti–human ZO-1 (33-9100; Invitrogen), mouse anti–human E-cadherin (U3254; Sigma-Aldrich), mouse monoclonal gp135 (a kind gift from George Ojakian, SUNY Downstate), rabbit anti-actin (A2066; Sigma-Aldrich), goat anti–human AQP2 (Santa Cruz Biotechnology, Santa Cruz, CA), monoclonal rat AQP1 (Thermo Fisher Scientific, Waltham, MA), mouse monoclonal γ-tubulin (T6557; Sigma-Aldrich), rabbit anti–mouse Par3 (07-330; Millipore, Billerica, MA), mouse anti–human aPKCλ (610207; BD Biosciences, Franklin Lakes, NJ), rabbit anti-GFP (A6455; Invitrogen). Rabbit anti–human Myo10 (SDIX, 2243.00.02) was used to confirm staining pattern in kidney (unpublished data).

Cells were prepared for immunofluorescence by fixation in 4% paraformaldehyde (Electron Microscopy Sciences, Hatfield, PA) in phosphate-buffered saline (PBS) for 30 min at room temperature; permeabilization for 10 min in 0.5% Triton-X (Sigma) in PBS; blocking for 1 h in 5% heat-inactivated goat serum (Sigma); and incubation in primary antibody (Myo10 [Sigma], E-cadherin, ZO-1, gp135; 0.5–1.0 μg/ml in 5% goat serum + 0.05% NaN_3) overnight at 4°C and in secondary antibody (1.0 μg/ml in goat serum) for 2 h at room temperature. Alexa Fluor 568 phalloidin (13 nM; Invitrogen Molecular Probes) and DAPI (200 nM; Sigma, D9542) were added with secondary antibody in 5% goat serum. Alexa Fluor 488 goat anti-rabbit or anti-mouse, and Alexa Fluor 568 goat anti–mouse immunoglobulin G (IgG; Invitrogen Molecular Probes) were used as secondary antibodies (1.0 μg/ml).

Immunofluorescence samples were imaged on an Olympus FluoView FV1000 confocal, inverted microscope (Center Valley, PA) using a PlanApo 60×/1.42 numerical aperture (NA) oil objective. The confocal microscope is equipped with diode lasers for 405, 559, and 635 nm, and an argon laser for 488 nm. For Z-stacks, 640 × 640 pixel, 0.44- to 0.5-μm slices were collected at 4.0 μs/pixel sampling speed in sequential line mode and using Kalman integration.

Samples were prepared for immunoblotting by lysis in SDS sample buffer with protease inhibitor cocktail, EDTA-free (Roche, Indianapolis, IN). Samples were either used immediately or flash frozen in liquid nitrogen and stored at –80°C. Samples were loaded onto 4–12% Bis-Tris gels (Invitrogen). Following gel electrophoresis, protein was transferred onto nitrocellulose membrane in an XCell

SureLock Electrophoresis system (Invitrogen), at 140 V for ~90 min using a PowerPac Basic power supply (BioRad, Hercules, CA). The membrane was blocked in 5% milk in TBST (50 mM Tris, 150 mM NaCl, 0.05% Tween 20, pH 7.5) for 30 min; this was followed by primary antibody (Myo10 [Sigma], actin; 0.8–1.0 µg/ml) in TBST overnight at 4°C. For chemiluminescence, horseradish peroxidase donkey anti-rabbit or donkey anti-mouse secondary antibodies (Jackson ImmunoResearch Laboratories, West Grove, PA) were used at 1:10,000 and incubated for 50 min in TBST. For LI-COR, membranes were incubated in anti–rabbit IgG IRDye700 (Rockland Immunochemicals, Gilbertsville, PA) at 1:10,000 in TBST and incubated for 45 min. Blots were imaged using the Odyssey Infrared Imaging System (LI-COR Biosciences, Lincoln, NE) and analyzed by measuring integrated intensities in the Odyssey applications software, version 3.0 (LI-COR Biosciences).

Immunohistochemistry

Protocols were approved by the Institutional Animal Care and Use Committee at University of North Carolina (UNC)-Chapel Hill. Five-micrometer paraffin-embedded kidney sections from C57BL/6 mice were a gift from Carie Facemire (UNC-Chapel Hill). Sections were incubated for 2 h at 60°C. Samples were washed twice with xylene, and then went through a graded series of ethanol to distilled water washes: 6 min in 100% ethanol, 5 min in 95% ethanol, 3 min in 70% ethanol, and 1 min in distilled water. Antigen retrieval was performed by decloaking in citrate buffer solution (pH 6; S1699; Dako, Carpinteria, CA) in a decloaking chamber (Biocare Medical, Concord, CA) heated at 120°C for 30 s, 90°C for 10 s, and room temperature for 20 min. Sections were blocked in 5% heat-inactivated goat serum for 1 h. Samples were incubated in 5–10 µg/ml primary antibody (Myo10 [Sigma], AQP1, AQP2) in 5% goat serum overnight at 4°C, which was followed by rinses in PBS and incubation in secondary antibody at 1 µg/ml in 5% goat serum for 2 h at room temperature.

Barrier assays: calcium-switch, TER, and paracellular flux

For calcium-switch assays, MDCK cells were plated in quadruplicate at 7.5×10^4 cells/well on 10-mm Transwell-Clear filters with 0.4-µm pore size (Corning, Corning, NY) in 0.5 ml complete media. MDCK cells were grown for at least 5 d until confluent. Cells were then incubated overnight at 37°C in low-calcium media: SMEM (Life Technologies) with 5% calcium-depleted fetal bovine serum, 100 U/ml penicillin–streptomycin, and 5 µM $CaCl_2$ to disrupt junctions, as previously described (Gumbiner and Simons, 1986). After overnight incubation, low-calcium media was replaced with complete normal-calcium media. For time-course experiments, samples were fixed in 4% paraformaldehyde at 0, 0.5, 2, 2.5, 4.5, 5.5, and 24 h for immunofluorescence microscopy. For TER assays, TER measurements of Transwell filters were taken at regular time intervals using an EndOhm-12 chamber and an EVOM epithelial voltohmmeter (WPI, Sarasota, FL). Paracellular flux of uncharged macromolecules was measured using 3.0-kDa fluorescein-conjugated dextran (Invitrogen) on 6- to 7-d monolayers (Van Itallie *et al.*, 2009). Transwell filters were preincubated for 30 min with Hank's balanced salt solution (without $CaCl_2$, $MgCl_2$, $MgSO_4$; Life Technologies) supplemented with 1.8 $CaCl_2$. FITC-dextran (0.3 mg/ml) was added to the apical compartment; after a 2-h incubation, samples were taken from the basolateral compartment. FITC-dextran concentrations were measured in replicate using the Synergy HT plate reader with Gen5 Data Analysis Software (BioTek, Winooski, VT). Sample concentrations were determined by plotting against a standard curve of known FITC-dextran concentrations using linear regression in Microsoft Excel (Redmond, WA).

Spindle angle and length measurements

MDCK cells were grown to confluence on glass coverslips. MDCK monolayers were fixed in 4% paraformaldehyde for 30 min, permeabilized with 0.5% Triton-X for 10 min, and blocked with 5% heat-inactivated goat serum. Cells were stained with DAPI (1:500) and anti-γ-tubulin (1:1000). Metaphase cells were identified by DAPI staining of condensed chromosomes located at the metaphase plate. Centrosomes were identified by γ-tubulin. Z-stacks (0.5-µm slice thickness) were collected by laser scanning confocal microscopy (UNC–Olympus Imaging Center). Z-stacks were imported into ImageJ, and for each centromere, the *z*-position was determined by measuring the plane of maximum fluorescence using the Plot z-axis profile function. The *z*-distance between two centromeres within a cell was calculated by the difference between *z*-positions. Then maximum *xy*-projections were generated from γ-tubulin Z-stacks. The projected *xy*-distance between two centromeres within a cell was measured, and given the *z*-distance (*z*) and projected *xy*-distance (*xy*), the spindle angle (α°) was calculated by the equation, $\alpha^\circ = \tan^{-1}(z/xy)$. Spindle angle is defined by 0° being horizontal or parallel to the coverslip. Spindle length was calculated by the Pythagorean theorem, spindle length = $\sqrt{[z^2 + (xy)^2]}$. Fifty metaphase cells were measured per condition. Statistical analysis was performed in GraphPad Prism 5 (La Jolla, CA).

Three-dimensional cysts

MDCK cells were grown in three-dimensional culture using a protocol modified from Jaffe *et al.* (2008). Trypsinized MDCK cells were resuspended at 0.5×10^4 cells/well in 40% Matrigel phenol-free (BD Biosciences, San Jose, CA), 1 mg/ml rat tail collagen I (Sigma-Aldrich), and 20 mM HEPES (pH 7.5) and plated on 10-mm Transwell filters. The gels were allowed to set for 30 min at 37°C before complete media was added. Three-dimensional cysts were grown for 6 d, then fixed in 4% paraformaldehyde as described above. For each experiment, random fields of view were imaged, and cysts were counted as having single or multiple lumens from these images. One hundred cysts were counted for each experiment per condition.

Statistical analysis

For steady-state TER and paracellular flux measurements, statistical analysis was determined using a two-tailed Student's *t* test with significance defined by p value < 0.01. For three-dimensional cysts, the average numbers of single lumens were compared between groups using one-way analysis of variance. If significant, post hoc comparisons using Tukey's method were performed. All statistical analyses were performed in GraphPad Prism 5. All error bars denote SEM.

ACKNOWLEDGMENTS

This research was supported by grants from the National Institutes of Health, National Institute on Deafness and Other Communication Disorders (DC03299) and National Heart, Lung, and Blood Institute (HL080166) to R.E.C., National Institute of Digestive and Kidney Diseases (NIDDK; DK061397) to A.S.F., and NIDDK predoctoral National Research Service Award fellowship 1F30DK089695-01 to K.C.L. We also acknowledge the support of the UNC–Olympus Imaging Center. We thank Nicholas Moss for his advice and suggestions and Michael Kerber for technical assistance with TIRF microscopy.

REFERENCES

Abouhamed M, Grobe K, San IV, Thelen S, Honnert U, Balda MS, Matter K, Bahler M (2009). Myosin IXa regulates epithelial differentiation and its deficiency results in hydrocephalus. Mol Biol Cell 20, 5074–5085.

Adams CL, Nelson WJ, Smith SJ (1996). Quantitative analysis of cadherin-catenin-actin reorganization during development of cell-cell adhesion. J Cell Biol 135, 1899–1911.

Almagro S *et al*. (2010). The motor protein myosin-X transports VE-cadherin along filopodia to allow the formation of early endothelial cell-cell contacts. Mol Cell Biol 30, 1703–1717.
Anderson JM, Van Itallie CM (2009). Physiology and function of the tight junction. Cold Spring Harb Perspect Biol 1, a002584.
Arganda-Carreras I, Fernandez-Gonzalez R, Munoz-Barrutia A, Ortiz-De-Solorzano C (2010). 3D reconstruction of histological sections: application to mammary gland tissue. Microsc Res Tech 73, 1019–1029.
Au JS, Puri C, Ihrke G, Kendrick-Jones J, Buss F (2007). Myosin VI is required for sorting of AP-1B-dependent cargo to the basolateral domain in polarized MDCK cells. J Cell Biol 177, 103–114.
Balda MS, Whitney JA, Flores C, Gonzalez S, Cereijido M, Matter K (1996). Functional dissociation of paracellular permeability and transepithelial electrical resistance and disruption of the apical-basolateral intramembrane diffusion barrier by expression of a mutant tight junction membrane protein. J Cell Biol 134, 1031–1049.
Bennett RD, Mauer AS, Strehler EE (2007). Calmodulin-like protein increases filopodia-dependent cell motility via up-regulation of myosin-10. J Biol Chem 282, 3205–3212.
Berg JS, Cheney RE (2002). Myosin-X is an unconventional myosin that undergoes intrafilopodial motility. Nat Cell Biol 4, 246–250.
Berg JS, Derfler BH, Pennisi CM, Corey DP, Cheney RE (2000). Myosin-X, a novel myosin with pleckstrin homology domains, associates with regions of dynamic actin. J Cell Sci 113, 3439–3451.
Bohil AB, Robertson BW, Cheney RE (2006). Myosin-X is a molecular motor that functions in filopodia formation. Proc Natl Acad Sci USA 103, 12411–12416.
Boller K, Vestweber D, Kemler R (1985). Cell-adhesion molecule uvomorulin is localized in the intermediate junctions of adult intestinal epithelial cells. J Cell Biol 100, 327–332.
Booth AG, Kenny AJ (1976). Proteins of the kidney microvillus membrane. Identification of subunits after sodium dodecylsulphate/polyacrylamide-gel electrophoresis. Biochem J 159, 395–407.
Breshears LM, Wessels D, Soll DR, Titus MA (2010). An unconventional myosin required for cell polarization and chemotaxis. Proc Natl Acad Sci USA 107, 6918–6923.
Bruewer M, Hopkins AM, Hobert ME, Nusrat A, Madara JL (2004). RhoA, Rac1, and Cdc42 exert distinct effects on epithelial barrier via selective structural and biochemical modulation of junctional proteins and F-actin. Am J Physiol Cell Physiol 287, C327–C335.
Capaldo CT, Macara IG (2007). Depletion of E-cadherin disrupts establishment but not maintenance of cell junctions in Madin-Darby canine kidney epithelial cells. Mol Biol Cell 18, 189–200.
Cereijido M, Robbins ES, Dolan WJ, Rotunno CA, Sabatini DD (1978). Polarized monolayers formed by epithelial cells on a permeable and translucent support. J Cell Biol 77, 853–880.
Claude P (1978). Morphological factors influencing transepithelial permeability: a model for the resistance of the zonula occludens. J Membr Biol 39, 219–232.
Cox D, Berg JS, Cammer M, Chinegwundoh JO, Dale BM, Cheney RE, Greenberg S (2002). Myosin X is a downstream effector of PI(3)K during phagocytosis. Nat Cell Biol 4, 469–477.
den Elzen N, Buttery CV, Maddugoda MP, Ren G, Yap AS (2009). Cadherin adhesion receptors orient the mitotic spindle during symmetric cell division in mammalian epithelia. Mol Biol Cell 20, 3740–3750.
Fanning AS, Van Itallie C, Anderson JM (2012). Zonula occludens (ZO)-1 and -2 regulate apical cell structure and the zonula adherens cytoskeleton in polarized epithelia. Mol Biol Cell 23, 577–590.
Friedman TB, Liang Y, Weber JL, Hinnant JT, Barber TD, Winata S, Arhya IN, Asher JH, Jr. (1995). A gene for congenital, recessive deafness DFNB3 maps to the pericentromeric region of chromosome 17. Nat Genet 9, 86–91.
Gonzalez-Mariscal L, Chavez de Ramirez B, Cereijido M (1985). Tight junction formation in cultured epithelial cells (MDCK). J Membr Biol 86, 113–125.
Gumbiner B, Simons K (1986). A functional assay for proteins involved in establishing an epithelial occluding barrier: identification of a uvomorulin-like polypeptide. J Cell Biol 102, 457–468.
Gumbiner B, Simons K (1987). The role of uvomorulin in the formation of epithelial occluding junctions. Ciba Found Symp 125, 168–186.
Hao Y, Du Q, Chen X, Zheng Z, Balsbaugh JL, Maitra S, Shabanowitz J, Hunt DF, Macara IG (2010). Par3 controls epithelial spindle orientation by aPKC-mediated phosphorylation of apical Pins. Curr Biol 20, 1809–1818.
Harris TJ, Tepass U (2010). Adherens junctions: from molecules to morphogenesis. Nat Rev Mol Cell Biol 11, 502–514.
Hartsock A, Nelson WJ (2008). Adherens and tight junctions: structure, function and connections to the actin cytoskeleton. Biochim Biophys Acta 1778, 660–669.
Hirokawa N, Heuser JE (1981). Quick-freeze, deep-etch visualization of the cytoskeleton beneath surface differentiations of intestinal epithelial cells. J Cell Biol 91, 399–409.
Hirokawa N, Keller TC, III, Chasan R, Mooseker MS (1983). Mechanism of brush border contractility studied by the quick-freeze, deep-etch method. J Cell Biol 96, 1325–1336.
Hirokawa N, Tilney LG (1982). Interactions between actin filaments and between actin filaments and membranes in quick-frozen and deeply etched hair cells of the chick ear. J Cell Biol 95, 249–261.
Ivanov AI (2008). Actin motors that drive formation and disassembly of epithelial apical junctions. Front Biosci 13, 6662–6681.
Ivanov AI, Bachar M, Babbin BA, Adelstein RS, Nusrat A, Parkos CA (2007). A unique role for nonmuscle myosin heavy chain IIA in regulation of epithelial apical junctions. PLoS One 2, e658.
Ivanov AI, Hopkins AM, Brown GT, Gerner-Smidt K, Babbin BA, Parkos CA, Nusrat A (2008). Myosin II regulates the shape of three-dimensional intestinal epithelial cysts. J Cell Sci 121, 1803–1814.
Ivanov AI, McCall IC, Parkos CA, Nusrat A (2004). Role for actin filament turnover and a myosin II motor in cytoskeleton-driven disassembly of the epithelial apical junctional complex. Mol Biol Cell 15, 2639–2651.
Jaffe AB, Kaji N, Durgan J, Hall A (2008). Cdc42 controls spindle orientation to position the apical surface during epithelial morphogenesis. J Cell Biol 183, 625–633.
Kaissling B, Kriz W (1992). Morphology of the loop of Henle, distal tubule, and collecting duct. In: Renal Physiology, Vol. 1, Handbook of Physiology, ed. E. E. Windhager, New York: Oxford University Press, 109–168.
Kerber ML, Cheney RE (2011). Myosin-X: a MyTH-FERM myosin at the tips of filopodia. J Cell Sci 124, 3733–3741.
Kerber ML, Jacobs DT, Campagnola L, Dunn BD, Yin T, Sousa AD, Quintero OA, Cheney RE (2009). A novel form of motility in filopodia revealed by imaging myosin-X at the single-molecule level. Curr Biol 19, 967–973.
Kovacs M, Wang F, Sellers JR (2005). Mechanism of action of myosin X, a membrane-associated molecular motor. J Biol Chem 280, 15071–15083.
Krasnow MA, Nelson WJ (2002). Tube morphogenesis. Trends Cell Biol 12, 351.
Kwon M, Godinho SA, Chandhok NS, Ganem NJ, Azioune A, Thery M, Pellman D (2008). Mechanisms to suppress multipolar divisions in cancer cells with extra centrosomes. Genes Dev 22, 2189–2203.
Liu XZ, Walsh J, Mburu P, Kendrick-Jones J, Cope MJ, Steel KP, Brown SD (1997). Mutations in the myosin VIIA gene cause non-syndromic recessive deafness. Nat Genet 16, 188–190.
Lu Q, Yu J, Yan J, Wei Z, Zhang M (2011). Structural basis of the myosin X PH1(N)-PH2-PH1(C) tandem as a specific and acute cellular PI(3,4,5)P(3) sensor. Mol Biol Cell 22, 4268–4278.
Madara JL (1998). Regulation of the movement of solutes across tight junctions. Annu Rev Physiol 60, 143–159.
Maddugoda MP, Crampton MS, Shewan AM, Yap AS (2007). Myosin VI and vinculin cooperate during the morphogenesis of cadherin cell-cell contacts in mammalian epithelial cells. J Cell Biol 178, 529–540.
Mangold S, Wu SK, Norwood SJ, Collins BM, Hamilton NA, Thorn P, Yap AS (2011). Hepatocyte growth factor acutely perturbs actin filament anchorage at the epithelial zonula adherens. Curr Biol 21, 503–507.
Mao Y, Tournier AL, Bates PA, Gale JE, Tapon N, Thompson BJ (2011). Planar polarization of the atypical myosin Dachs orients cell divisions in *Drosophila*. Genes Dev 25, 131–136.
Martin-Belmonte F, Gassama A, Datta A, Yu W, Rescher U, Gerke V, Mostov K (2007). PTEN-mediated apical segregation of phosphoinositides controls epithelial morphogenesis through Cdc42. Cell 128, 383–397.
Mashanov GI, Tacon D, Peckham M, Molloy JE (2004). The spatial and temporal dynamics of pleckstrin homology domain binding at the plasma membrane measured by imaging single molecules in live mouse myoblasts. J Biol Chem 279, 15274–15280.
McCarthy KM, Francis SA, McCormack JM, Lai J, Rogers RA, Skare IB, Lynch RD, Schneeberger EE (2000). Inducible expression of claudin-1-myc but not occludin-VSV-G results in aberrant tight junction strand formation in MDCK cells. J Cell Sci 113, 3387–3398.
McConnell RE, Benesh AE, Mao S, Tabb DL, Tyska MJ (2011). Proteomic analysis of the enterocyte brush border. Am J Physiol Gastrointest Liver Physiol 300, G6914–G926.

McNeil E, Capaldo CT, Macara IG (2006). Zonula occludens-1 function in the assembly of tight junctions in Madin-Darby canine kidney epithelial cells. Mol Biol Cell 17, 1922–1932.
Muller T *et al*. (2008). MYO5B mutations cause microvillus inclusion disease and disrupt epithelial cell polarity. Nat Genet 40, 1163–1165.
Nagy S, Ricca BL, Norstrom MF, Courson DS, Brawley CM, Smithback PA, Rock RS (2008). A myosin motor that selects bundled actin for motility. Proc Natl Acad Sci USA 105, 9616–9620.
Nielsen S, Frokiaer J, Marples D, Kwon TH, Agre P, Knepper MA (2002). Aquaporins in the kidney: from molecules to medicine. Physiol Rev 82, 205–244.
Perez-Moreno M, Jamora C, Fuchs E (2003). Sticky business: orchestrating cellular signals at adherens junctions. Cell 112, 535–548.
Pi X, Ren R, Kelley R, Zhang C, Moser M, Bohil AB, Divito M, Cheney RE, Patterson C (2007). Sequential roles for myosin-X in BMP6-dependent filopodial extension, migration, and activation of BMP receptors. J Cell Biol 179, 1569–1582.
Plantard L, Arjonen A, Lock JG, Nurani G, Ivaska J, Stromblad S (2010). PtdIns(3,4,5)P is a regulator of myosin-X localization and filopodia formation. J Cell Sci 123, 3525–3534.
Qin Y, Meisen WH, Hao Y, Macara IG (2010). Tuba, a Cdc42 GEF, is required for polarized spindle orientation during epithelial cyst formation. J Cell Biol 189, 661–669.
Roland JT, Bryant DM, Datta A, Itzen A, Mostov KE, Goldenring JR (2011). Rab GTPase-Myo5B complexes control membrane recycling and epithelial polarization. Proc Natl Acad Sci USA 108, 2789–2794.
Schluter MA, Pfarr CS, Pieczynski J, Whiteman EL, Hurd TW, Fan S, Liu CJ, Margolis B (2009). Trafficking of Crumbs3 during cytokinesis is crucial for lumen formation. Mol Biol Cell 20, 4652–4663.
Schneeberger EE, Lynch RD (2004). The tight junction: a multifunctional complex. Am J Physiol Cell Physiol 286, C1213–C1228.
Schoenenberger CA, Zuk A, Zinkl GM, Kendall D, Matlin KS (1994). Integrin expression and localization in normal MDCK cells and transformed MDCK cells lacking apical polarity. J Cell Sci 107, 527–541.
Schoumacher M, Goldman RD, Louvard D, Vignjevic DM (2010). Actin, microtubules, and vimentin intermediate filaments cooperate for elongation of invadopodia. J Cell Biol 189, 541–556.
Shen L, Black ED, Witkowski ED, Lencer WI, Guerriero V, Schneeberger EE, Turner JR (2006). Myosin light chain phosphorylation regulates barrier function by remodeling tight junction structure. J Cell Sci 119, 2095–2106.
Shen L, Weber CR, Raleigh DR, Yu D, Turner JR (2011). Tight junction pore and leak pathways: a dynamic duo. Annu Rev Physiol 73, 283–309.
Shewan AM, Maddugoda M, Kraemer A, Stehbens SJ, Verma S, Kovacs EM, Yap AS (2005). Myosin 2 is a key Rho kinase target necessary for the local concentration of E-cadherin at cell-cell contacts. Mol Biol Cell 16, 4531–4542.
Shin K, Straight S, Margolis B (2005). PATJ regulates tight junction formation and polarity in mammalian epithelial cells. J Cell Biol 168, 705–711.
Smutny M, Cox HL, Leerberg JM, Kovacs EM, Conti MA, Ferguson C, Hamilton NA, Parton RG, Adelstein RS, Yap AS (2010). Myosin II isoforms identify distinct functional modules that support integrity of the epithelial zonula adherens. Nat Cell Biol 12, 696–702.
Sousa AD, Cheney RE (2005). Myosin-X: a molecular motor at the cell's fingertips. Trends Cell Biol 15, 533–539.
Stevenson BR, Siliciano JD, Mooseker MS, Goodenough DA (1986). Identification of ZO-1: a high molecular weight polypeptide associated with the tight junction (zonula occludens) in a variety of epithelia. J Cell Biol 103, 755–766.
Sun Y, Sato O, Ruhnow F, Arsenault ME, Ikebe M, Goldman YE (2010). Single-molecule stepping and structural dynamics of myosin X. Nat Struct Mol Biol 17, 485–491.
Tokuo H, Mabuchi K, Ikebe M (2007). The motor activity of myosin-X promotes actin fiber convergence at the cell periphery to initiate filopodia formation. J Cell Biol 179, 229–238.
Toyoshima F, Nishida E (2007). Integrin-mediated adhesion orients the spindle parallel to the substratum in an EB1- and myosin X-dependent manner. EMBO J 26, 1487–1498.
Umeda K, Matsui T, Nakayama M, Furuse K, Sasaki H, Furuse M, Tsukita S (2004). Establishment and characterization of cultured epithelial cells lacking expression of ZO-1. J Biol Chem 279, 44785–44794.
Umeki N, Jung HS, Sakai T, Sato O, Ikebe R, Ikebe M (2011). Phospholipid-dependent regulation of the motor activity of myosin X. Nat Struct Mol Biol 18, 783–788.
Van Itallie CM, Anderson JM (2006). Claudins and epithelial paracellular transport. Annu Rev Physiol 68, 403–429.
Van Itallie CM, Fanning AS, Bridges A, Anderson JM (2009). ZO-1 stabilizes the tight junction solute barrier through coupling to the perijunctional cytoskeleton. Mol Biol Cell 20, 3930–3940.
Vasioukhin V, Bauer C, Yin M, Fuchs E (2000). Directed actin polymerization is the driving force for epithelial cell-cell adhesion. Cell 100, 209–219.
Watanabe TM, Tokuo H, Gonda K, Higuchi H, Ikebe M (2010). Myosin-X induces filopodia by multiple elongation mechanism. J Biol Chem 285, 19605–19614.
Weber KL, Sokac AM, Berg JS, Cheney RE, Bement WM (2004). A microtubule-binding myosin required for nuclear anchoring and spindle assembly. Nature 431, 325–329.
Wei Z, Yan J, Lu Q, Pan L, Zhang M (2011). Cargo recognition mechanism of myosin X revealed by the structure of its tail MyTH4-FERM tandem in complex with the DCC P3 domain. Proc Natl Acad Sci USA 108, 3572–3577.
Woolner S, O'Brien LL, Wiese C, Bement WM (2008). Myosin-10 and actin filaments are essential for mitotic spindle function. J Cell Biol 182, 77–88.
Yonezawa S, Yoshizaki N, Sano M, Hanai A, Masaki S, Takizawa T, Kageyama T, Moriyama A (2003). Possible involvement of myosin-X in intercellular adhesion: importance of serial pleckstrin homology regions for intracellular localization. Dev Growth Differ 45, 175–185.
Zhang H, Berg JS, Li Z, Wang Y, Lang P, Sousa AD, Bhaskar A, Cheney RE, Stromblad S (2004). Myosin-X provides a motor-based link between integrins and the cytoskeleton. Nat Cell Biol 6, 523–531.
Zhang J, Betson M, Erasmus J, Zeikos K, Bailly M, Cramer LP, Braga VM (2005). Actin at cell-cell junctions is composed of two dynamic and functional populations. J Cell Sci 118, 5549–5562.